Journal of Luminescence 158 (2015) 306–312

Contents lists available at ScienceDirect

Journal of Luminescence

journal homepage: www.elsevier.com/locate/jlumin

Green emission from ZnO–MgO nanocomposite due to Mg diffusion at the interface

K. Sowri Babu *, A. Ramachandra Reddy, K. Venugopal Reddy

Department of Physics, National Institute of Technology Warangal, Warangal 506004, AP, India

ARTICLE INFO

Article history:
Received 17 May 2014
Received in revised form
2 October 2014
Accepted 14 October 2014
Available online 23 October 2014

Keywords:
ZnO nanocrystals
Photoluminescence
MgO
Nanocomposites

ABSTRACT

The origin and electronic transitions responsible for green emission observed from ZnO–MgO nanocomposite are investigated. The photoluminescence (PL) spectrum of ZnO–MgO nanocomposite annealed at 600 °C showed only a sharp and intense UV emission peak centered at 396 nm. As the annealing temperature increased from 600 °C to 1000 °C, the green emission positioned at 503 nm is emerged and its intensity enhanced gradually and reached maximum value at 900 °C and then decreased at 1000 °C. It is observed that both UV and green emission intensities are enhanced with variation of atomic ratio (Zn/Mg = 1.52, 0.50, 0.30, 0.21, 0.15). Our experiments confirmed that the enhancement of green emission intensity is due to the formation of oxygen vacancies (V_o) due to Mg doping at the interface of ZnO and MgO. This experimental observation is in good agreement with the recent theoretical predictions which states that Mg doping in ZnO lowers the formation energies of oxygen vacancies (V_o) and zinc interstitials (Zn_i) significantly. PL excitation and emission spectra analysis reveals that excited state for both UV and green emissions is same and lies 0.24 eV below the conduction band of ZnO. Hence, the green emission is attributed to the transition of an electron form the shallow donor (defect level of Zn_i) to the deep acceptor (defect level of V_o).

1. Introduction

Among the II–VI metal oxide semiconductors, ZnO has been investigated widely for its use in short wavelength opto-electronic devices due to its wide and direct band gap of 3.37 eV and large exciton binding energy of 60 meV at room temperature [1]. The exciton binding energy of ZnO is two times higher than the exciton binding energy of GaN (~25 meV) and room temperature thermal energy (K_BT) ensures the stable exciton emission even at room temperature. Because of these unique properties, ZnO finds potential applications in opto-electronic and electronic devices. The high emission efficiency of ZnO makes it as a promising semiconductor material for solid state white lighting [2]. Further, ZnO is used as a transparent conductor in solar cells [3,4], UV absorbing materials in sunscreens [5], active material in varistors [6] and transparent transistor in liquid crystal displays [7]. Apart from these applications, ZnO is also an important material for spintronic applications [8]. The ZnO nanostructures generally show two emission bands; one positioned in the UV region termed as near band edge emission (NBE) and the other positioned in the visible region (500–530 nm) called green emission or deep level emission [9]. The origin of this green luminescence of ZnO is in dispute for a long time. It has been assigned to the singly ionized oxygen vacancies [10], transition of an electron from the conduction band to a deep trap [9], zinc vacancy (V_{Zn}) creation of Zn vacancies (V_{Zn}) [11], surface states [12], and then formation of Cu dopants at Zn sites (Cu_{Zn}) [13]. To improve the luminescence property, the surfaces of ZnO nanostructures were passivated by various types of shell materials such as SiO_2, ZnS, SnO_2, Al_2O_3 and MgO [14–18]. Bera et al. reported ZnO–MgO nanocomposite as an ideal nanocomposite [19]. The ZnO–MgO heterostructures, may be useful as chemical sensors, optical devices and scanning probes in addition to providing a reliable heterojunction material to study quantum confinement effects [20]. Moreover, ZnO–MgO nanocomposites have optical properties which can be potentially useful for bio-imaging applications [21]. ZnO nanoparticles coated with MgO have also shown enhanced gas sensing property [22]. Many authors reported that the near band edge (NBE) emission of ZnO nanoparticles has been enhanced by forming ZnO–MgO nanocomposites [1,23–27]. Some authors also found an intense green emission from ZnO–MgO nanocomposites [19,28]. Bang et al. reported that an enhanced and stable green emission from ZnO nanoparticles and attributed to surface segregation of Mg [28]. Semiconductor nanocrystals emitting visible light may be useful in fluorescent probes in bio-labeling and also in visible light display applications [13].

* Corresponding author. Tel.: +91 870 2462593; fax: +91 870 2462010.
E-mail address: sowribabuk@gmail.com (K. Sowri Babu).

http://dx.doi.org/10.1016/j.jlumin.2014.10.027
0022-2313/

In the present study, the effect of Mg concentration and annealing temperature on the PL emission of ZnO–MgO nanocomposites is investigated. The formation of ZnO–MgO nanocomposites has been confirmed by XRD and HR-TEM. The intensity of the UV emission positioned at 396 nm enhanced with increase of Mg concentration. As the temperature increased from 600 °C to 1000 °C, the green emission intensity enhanced remarkably until 900 °C and decreased afterwards. The reasons for the intensity variations of green emission intensity are discussed in detail. The experiments indicated that diffusion of Mg atoms at the interface of ZnO and MgO give rise to intense green emission. It is also found that the green emission is attributed to the transition of an electron form the shallow donor (defect level of Zn_i) to the deep acceptor (defect level of V_o).

2. Experimental procedure

2.1. Synthesis of ZnO–MgO nanocomposite

The preparation of ZnO nanoparticles is same as described elsewhere [29]. To prepare ZnO–MgO nanocomposite powders, stoichiometric quantities of Mg $(NO_3)_2.6H_2O$ and NaOH were dissolved in deionized water in separate beakers and stirred vigorously for sufficient time. In the next step, NaOH solution was slowly added to the Mg $(NO_3)_2 \cdot 6H_2O$ aqueous solution drop wise along the walls of the beaker for 30 min while stirring and the temperature of the solution was maintained at 60 °C. To this solution, one gram of the as prepared ZnO was added and stirring was continued for two more hours and aged for four hours. Subsequently, samples were filtered and washed with deionized water and ethanol three times and dried in an oven at 100 °C for 8 h. Sufficient number of samples were prepared with different concentrations of Mg such as 0.05 M, 0.15 M, 0.25 M, 0.35 M and 0.5 M or atomic ratio's (Zn/Mg) 1.52, 0.50, 0.30, 0.21, 0.15) to study the structural and optical properties of ZnO–MgO nanocomposite in detail. These five samples are labeled as ZM1, ZM2, ZM3, ZM4 and ZM5. The dried samples were annealed in a programmable muffle furnace at 600 °C at a rate of 2 °C/min and allowed to stay for one hour at each temperature. To investigate the effect of annealing temperature on structural and optical properties of ZnO–MgO nanocomposite, sample prepared with 0.25 M (ZM3) of Mg was annealed at 700, 800, 900 and 1000 °C with the same heating rate as used above.

2.2. Characterization

The structural analysis of samples was carried out by X-ray diffractometer (Bruker D8) equipped with Cu Kα radiation (λ= 1.5406 Å). The morphology, crystallite size and elemental analysis of the samples were probed by High Resolution-Transmission Electron Microscope (HR-TEM: model Tecnai G2 200 kV). The absorption was measured using Thermo Scientific UV–vis absorption spectrometer. The PL measurements were performed using Jobin Yuon spectrofluorometer containing 450 W Xenon arc lamp as source of excitation.

3. Results and discussion

3.1. XRD analysis

The X-Ray diffraction patterns of ZnO and ZnO–MgO nanocomposite powders prepared with different concentrations of Mg are shown in Fig. 1. The diffraction peaks corresponding to the (100), (002), (101), (102), (110) and (103) planes confirmed the hexagonal wurtzite structure of ZnO nanocrystals. All the samples ZM1, ZM2 and ZM3 exhibited a diffraction peak centered at around 43.05° of

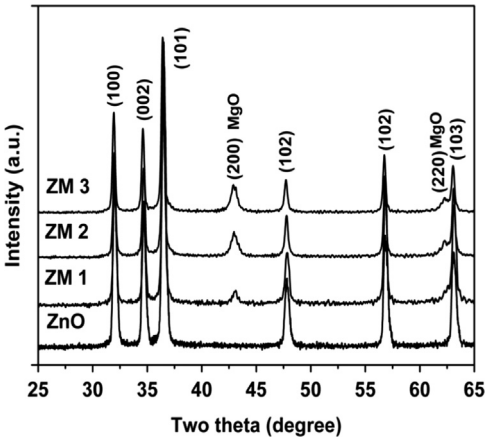

Fig. 1. The XRD patterns of ZnO and ZM1, ZM2 and ZM3 nanocomposites prepared with different Mg concentrations and annealed at 600 °C.

2θ value. This diffraction peak corresponds to the (200) reflection plane of the cubic MgO phase. Further, the diffraction peaks of ZnO are shifted gradually towards the lower angle side with increase of Mg concentration. A shift of 0.10° of (101) diffraction plane towards lower angle side is observed with change in Mg concentration from 0.05 to 0.25 M. To know the reason for this shift, lattice parameters (a and c) and volume of the unit cell of hexagonal ZnO structure are also calculated using appropriate formulas. There is a little increase in 'a', 'c' and volume of the unit cell values as the Mg concentration increases. It indicates the expansion of unit cell of ZnO with increase of Mg concentration. Hence, it is evident that ZnO nanocrystals are experiencing tensile strain with increase of Mg concentration. Similar kind of results have also been observed in Mn/Cu/Fe-doped and Co-doped ZnS NWs/ZnO QDs@SiO_2core/shell nanostructures [30] and also in CdTe/ZnSe core/shell nanostructures [31]. Generally, the diffraction peaks shift towards higher angle side with doping of Mg in ZnO due to the smaller ionic radius of Mg (0.66 Å) compared to Zn (0.74 Å). However, such a shift in the diffraction peaks towards higher angle is absent in these samples. The absence of the shift of the diffraction peaks towards higher angle side confirmed that Mg neither diffused nor doped into ZnO nanocrystals at an annealing temperature of 600 °C. The relatively small shift observed in this study indicates that perfect core/shell structure is not formed. However, the surfaces of ZnO nanocrystals may be covered with MgO. The formation of MgO coating on ZnO has been confirmed from the HR-TEM analysis of these samples. Further, average crystallite size values are calculated for all the samples using Debye Scherer formula.

$$D = \frac{0.9\lambda}{\beta \cos \theta}$$

where D is the diameter of grain size (in Å), β is the FWHM of the particular peak in radians, θ is the Braggs angle and λ (1.5405 Å) is the wavelength of x-rays used. Table 1 shows the various structural parameters of the samples. Table 1 shows that the crystallite size increases as the Mg concentration in the ZnO–MgO nanocomposite increases. The enhancement in the crystallite size may be due to the MgO coating over the ZnO nanocrystals surface. As the Mg concentration in the ZnO–MgO nanocomposite increases, thickness of the MgO attached to ZnO may also increases and hence there is an increase in crystallite size.

3.2. HR-TEM analysis

The ZnO–MgO nanocomposite is further analyzed with HR-TEM. Fig. 2(a) shows the HR-TEM image of ZM3 annealed at

Table 1
The structural parameters of ZM3 nanocomposite with different concentrations of Mg.

Sample name	Angle (2θ) hkl (100)	Crystallite size (nm)	Lattice parameter (nm)		Volume (V)= $a^2c\ \sin(60^\circ)$ (nm^3)
			a	C	
ZnO	32.0246	22	0.3224	0.5584	0.05029
ZM1	32.0143	25	0.3225	0.5586	0.05033
ZM2	31.9866	27	0.3228	0.5591	0.05046
ZM3	31.9290	28	0.3233	0.5601	0.05073

600 °C. This picture clearly shows the intimate contact between ZnO and MgO and confirms the formation of ZnO–MgO nanocomposite. Fig. 2(b) shows the HR-TEM image of the same sample but at higher resolutions. The lattice fringes of ZnO nanocrystals are not visible at this resolution may be due to the capping of ZnO nanoparticles with MgO. The inset of Fig. 2(b) shows the electron diffraction pattern of the ZnO–MgO nanocomposite annealed at 600 °C. This picture shows large number of diffraction spots distributed randomly. This random electron diffraction pattern may be due to the overlapping of electron diffraction patterns of ZnO and MgO. It indicates that MgO covers the surfaces of ZnO nanoparticles at 600 °C. Fig. 2(c) and (d) shows the pictures of ZM3 annealed at 900 °C and inset of Fig. 2(d) shows the electron diffraction pattern of the same sample. Fig. 2(b) shows that at 900 °C, ZnO and MgO nanocrystals have grown individually but there is an intimate contact between ZnO and MgO nanocrystals. Fig. 2(d) shows the lattice fringes of ZnO nanocrystals at same resolution used for the sample annealed at 600 °C. The distance between the lattice planes shown in Fig. 2(d) is 0.26 nm which is in good agreement with the XRD data of (002) plane of ZnO hexagonal wurtzite structure. The electron diffraction pattern shown in Fig. 2(d) exhibits diffraction spots arranged in concentric circles. It indicates ZnO nanocrystals are not covered by MgO but doped in ZnO. As a result of it, HR-TEM pictures of these samples shows lattice planes clearly. The TEM Energy dispersive spectroscopy (EDS) analysis of ZnO showed that there is no impurity present in the sample. It can be seen that Fig. 2(e) and (f) shows the EDS spectra of ZnO nanocrystals and ZnO–MgO nanocomposite. Fig. 2(f) shows the signals of Zn, O and Mg elements clearly and presence of other elements such as C and Cu are due to the carbon coated copper grid used for TEM analysis.

3.3. PL analysis

3.3.1. Effect of Mg concentration and annealing temperature

All the PL spectra were acquired with an excitation wavelength of 353 nm and the reason for choosing this excitation wavelength and origin of other peaks at 453 nm and 633 nm can be found elsewhere [32]. Fig. 3 shows the room temperature PL emission spectra of ZM1, ZM2 ZM3 and ZM4 nanocomposites annealed at 600 °C. The PL of ZnO nanoparticles showed only a sharp and intense UV emission positioned at 396 nm when annealed at 600 °C [32]. There is no deep level emission or green emission from ZnO nanocrystals when annealed at 600 °C. It is observed that the intensity of UV peak positioned at 396 nm enhanced with increase of Mg concentration until 0.25 M and there is no change in the intensity beyond this concentration. This is due to the fact that, if all the surface states are passivated; further enhancement in the MgO content brings no change in UV emission intensity [23]. Fig. 4 shows the PL spectra of ZM3 nanocomposite annealed at temperatures of 600 °C, 700 °C, 800 °C, 900 °C and 1000 °C. There is no green emission from ZM3 nanocomposite when annealed at 600 °C. However, with increase of annealing temperature up to 900 °C, the intensity of green emission positioned at 503 nm increased greatly and then decreased for further increase in temperature to 1000 °C. The intensity of green emission at 900 °C is nearly 18 times higher than its intensity at 700 °C. Very recently, we have observed that intensity of green emission positioned at 533 nm from pristine ZnO nanocrystals enhanced with increase of annealing temperature [33] but its maximum intensity is three times smaller than the intensity of UV emission peak. Kim et al. observed an intense green emission from MgO/ZnO core/shell nanowires and attributed it to the overlapping of green emissions from MgO and ZnO [34]. Hence the role of MgO and its contribution to the intense green emission observed in this study need to be understood.

3.3.2. Effect of Mg concentration and MgO on green emission

To understand the MgO contribution to green emission, MgO nano powder was prepared by the same method described above and its PL was recorded. Fig. 5. shows that MgO did not exhibit any emission peaks except a peak at 453 nm when excited with 353 nm wavelength. This result proved that MgO shell did not contributed to the green emission observed from ZnO–MgO nanocomposite. Mostly, the green emission from ZnO nanoparticles has been attributed to the singly ionized oxygen vacancies [35–37]. Our very recent results also support that green emission from pristine ZnO nanocrystals is due to the singly ionized oxygen vacancies [33]. To confirm this, ZM3 nanocomposite is annealed in the presence of oxygen gas. The PL of spectrum of ZM3 annealed in oxygen and in air are shown in Fig. 6. It shows only UV emission peak positioned at 396 nm or in other words, green emission is completely quenched when annealed in oxygen atmosphere. It confirmed that green emission observed from ZM3 nanocomposite is due to the oxygen vacancies present in the sample. Hence, the enhancement of the green emission can be attributed to increase in the oxygen vacancy related defect density. To verify the effect of Mg concentration on green emission, ZnO–MgO nanocomposites were prepared with different Mg concentrations and annealed at 900 °C. Three samples are prepared with low, medium and high concentrations of Mg to obtain ZnO–MgO nanocomposite. The PL spectra of these ZnO–MgO nanocomposites are also shown in Fig. 5. As can be seen from the plot, the green emission intensity increased with increase of Mg concentration. However, there is no appreciable change in the intensity of green emission for samples prepared with 0.25 and 0.50 M. This result indicates that there exists a critical concentration beyond which it has no influence on the intensity of green emission. It also indicates that green emission may be induced by the interface formed between ZnO and MgO. Lee et al. observed very little enhancement in the green emission intensity after ZnO nanoparticles coated with MgO and they attributed it to lattice mismatch between ZnO and MgO [38]. Some authors reported that the strain at the interface also generates the oxygen vacancies and hence there will be enhancement in the green emission intensity [39].

3.3.3. XRD analysis

To understand the effect of strain at the interface on green luminescence, the samples annealed at different temperatures were analyzed with the XRD technique to have an insight into the structural changes at high temperatures. Fig. 7 shows the XRD patterns of ZnO–MgO nanocomposite (ZM3) annealed in air at different temperatures from 600 to 1000 °C. The strain in the samples is calculated using Williamson–Hall analysis by simplified integral breadth method for ZnO and ZnO–MgO nanocomposite [40]. The integral breadth (β) defined as the ratio between peak area and the intensity maxima for both size and strain broadened profile, is given by

$$\beta^* = 1/D + 2\varepsilon s(\text{in } \sin\ \theta \text{ scale}) \quad (1)$$

where D is the average particle diameter, ε is the strain, $\beta^* = \beta \cos\theta/\lambda$, and $s = 2 \sin\theta/\lambda$. The average particle diameters were obtained from this analysis. The inverse of intercept gives the particles size

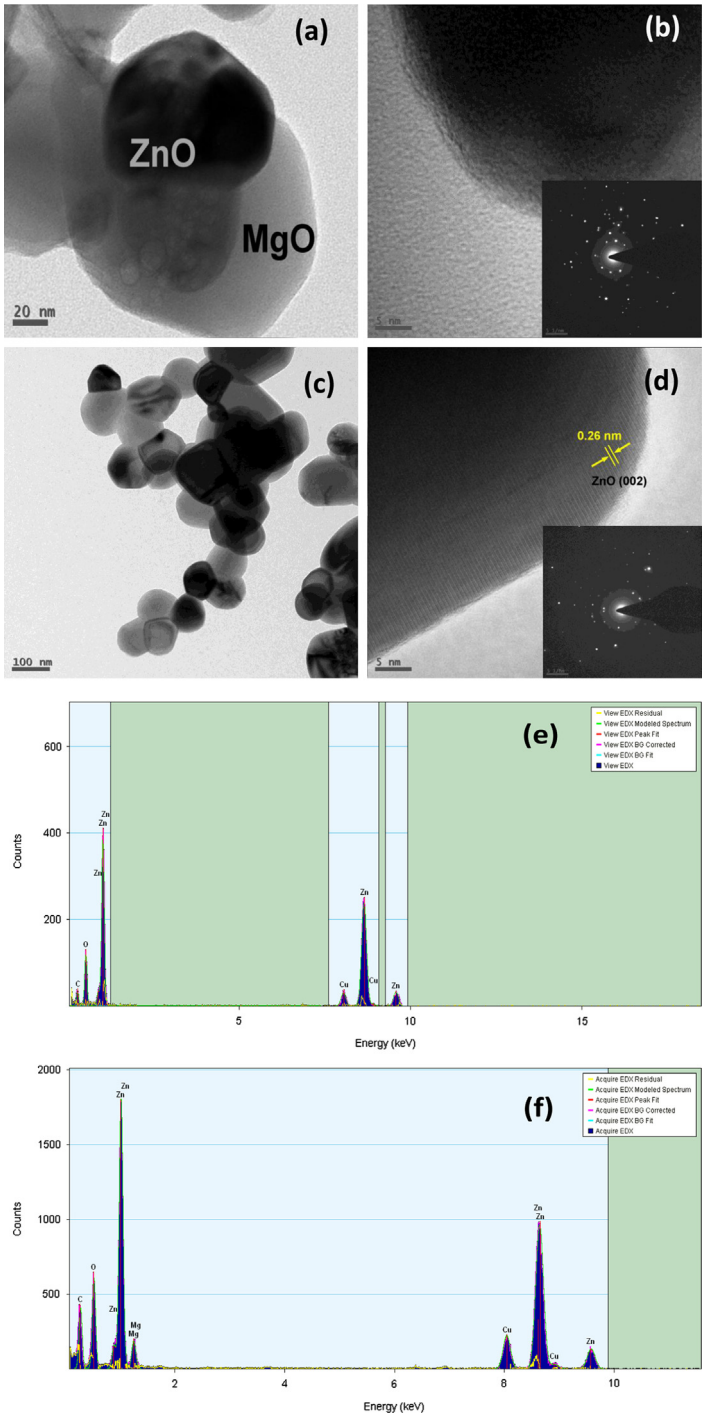

Fig. 2. The HR-TEM images (a) and (b) of ZM3 annealed at 600 °C, ZM3 annealed at (c) and (d) 900 °C and EDS spectra of (e) ZnO and (f) ZnO–MgO nanocomposite.

and slope of the linear fit gives the strain. It is observed that the slope of the W–H plots for ZM3 decreased gradually as the temperature increased from 600 °C to 1000 °C. It indicates that strain decreased monotonously as the temperature increased from 600 °C to 1000 °C. It is contrary to the variation in intensity of green emission which increased first until 900 °C and decreased at 1000 °C. Hence, it can be concluded that green emission is not due to the strain at the interface. The average crystallite size of the ZnO nanocrystals decreased as the temperature increased from 600 to 1000 °C and it is evident from the broadening of the XRD diffraction peaks. The decrease in the crystallite size may be due to the Mg doping at higher annealing temperatures. The lattice parameters '*a*', '*c*' and volume of the unit cell are calculated using the XRD data and are shown in Table 2. As can be seen from Table 2, the position of diffraction peak of ZnO–MgO nanocomposite is found to be shifted gradually towards higher angle side from $2\theta = 31.9290^{\circ}$ to $2\theta = 31.9820^{\circ}$ with increase of annealing temperature from 600 to 900 °C. The lattice parameter '*c*' and the unit cell volume decreases as the temperature increases from 600 °C to 900 °C. The decrease of the lattice parameter and volume of the unit cell suggests that Mg^{2+} is incorporated into the ZnO host lattice and substitutes for Zn^{2+}, since the ionic radius 0.066 nm of Mg^{2+} is smaller than that 0.074 nm of Zn^{2+} [41]. This is due to the fact that, thermal diffusion of Mg atoms at the ZnO–MgO interface takes place for temperatures

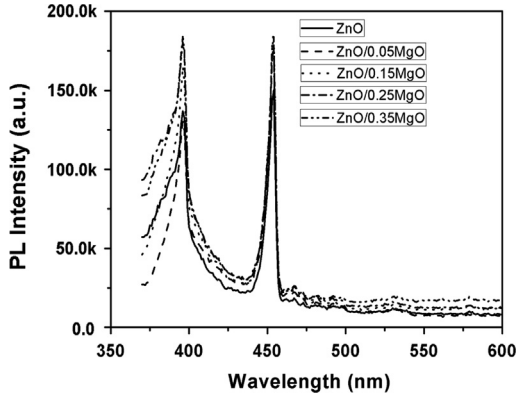

Fig. 3. The PL spectra of ZnO and ZM3 nanocomposite at 600 °C.

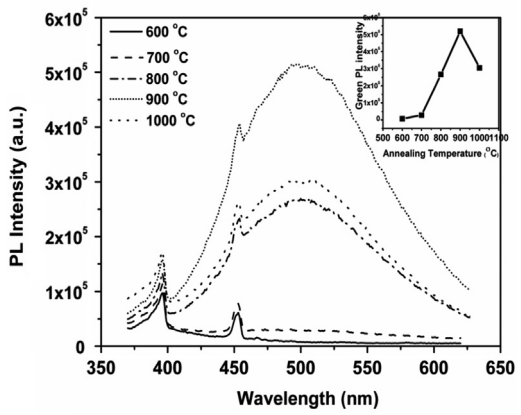

Fig. 4. The PL spectra of ZM3 nanocomposites annealed at various temperatures from 600 to 1000 °C and the inset displays the intensity variation of green emission with increase in annealing temperature.

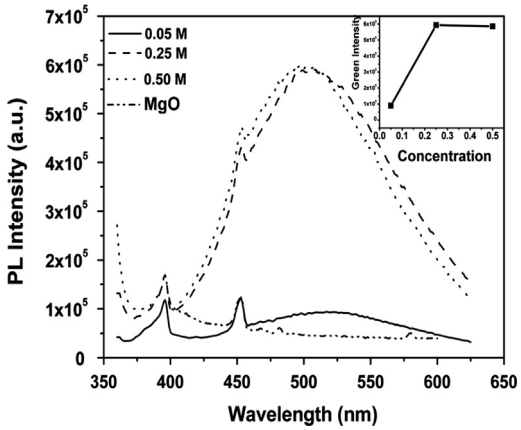

Fig. 5. The PL spectrum of ZM3 nanocomposites with different Mg concentrations and PL spectrum of MgO. The inset shows the intensity variation of green emission with Mg concentrations.

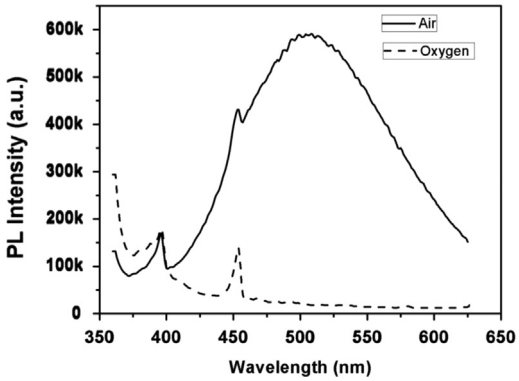

Fig. 6. The PL spectra of ZM3 nanocomposite annealed in air and oxygen atmosphere.

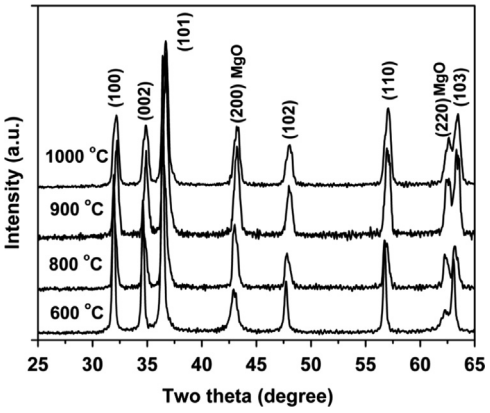

Fig. 7. (a) XRD patterns of ZM3 nanocomposites annealed at various temperatures, and (b) the variations of 2θ value of (101) plane and green emission intensities with increase of temperature from 600 to 1000 °C.

Table 2
The structural parameters of ZM3 nanocomposite with annealing temperature.

Annealing temperature (°C)	Angle (2θ) hkl (100)	Crystallite size (nm)	Lattice parameter (nm)		Volume (V)= $a^2c\sin(60°)$ (nm^3)
			a	c	
600	31.9290	28	0.3233	0.5601	0.05073
800	32.1318	16	0.3214	0.5566	0.04980
900	32.1705	18	0.3210	0.5560	0.04962
1000	32.9820	20	0.3228	0.5592	0.05048

greater than 700 °C [42]. To confirm this, UV–vis absorption spectra of these powders are also recorded and shown in Fig. 8. The absorption peak is shifted to lower wavelength side as the temperature increases from 600 °C to 900 °C. These results confirmed that Mg^{2+} is incorporated into the ZnO host lattice and substitutes for Zn^{2+}. Hence, it is believed that green emission may be due to the Mg diffusion into ZnO at the interface of ZnO and MgO. This result is in good agreement with the theoretical predictions of Dutta et al. They predicted that Mg doping significantly lowers the formation energies of oxygen vacancy (V_o) and zinc interstitials (Zn_i) [43]. The formation energies for different defects with Mg substitution in place of Zn are shown in Table 3. These results infer that the Mg atoms substitution in place of ZnO created deep trap levels in the band gap of ZnO. The charge carriers were trapped at these oxygen vacancy defect levels and give rise to the intense green emission.

Further, the lattice parameter 'c' and the unit cell volume of ZnO increased with increase in temperature to 1000 °C. It may be the indication that Mg^{2+} might diffused out from the ZnO nanocrystals at 1000 °C. In the view of the increase in particle size and unit cell volume, absorption spectrum should exhibit a red-shift. But Fig. 8 shows the absorption spectrum is further blue-shifted as the temperature increased to 1000 °C. From Table 3 it can be seen that the formation energy of interstitial zinc (Zn_i) is lower than compared to zinc vacancy (V_{Zn}). Hence, there is a possibility for the formation oI_{Zn} Zn_i f rather than V_{Zn} defects at 1000 °C. As a result of it the volume of the unit cell enhanced at this annealing temperature. The decrease of XRD peak intensities

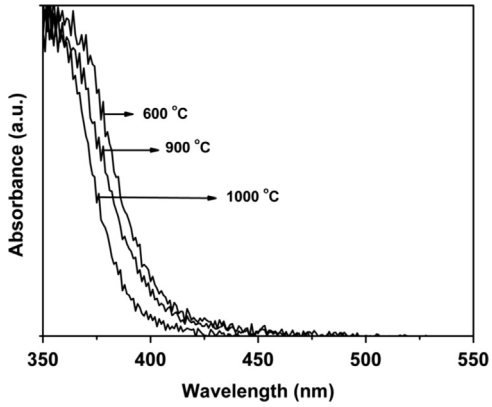

Fig. 8. UV–vis absorption spectra of ZM3 nanocomposite annealed at different temperatures.

Table 3
The formation energies of various defects in Mg-doped ZnO nanocrystals under various conditions.

Possible Mg sites	Formation energy (eV)	Condition
$Zn_{Mg}+V_{Zn}$	3.51	Zinc rich
$Zn_{Mg}+V_o$	2.40	Oxygen rich
$Zn_{Mg}+Zn_i$	1.35	Zinc rich

may be due to the worsening of the crystal quality due to the formation of Zn_i at 1000 °C. However, the absorption spectrum is still blue-shifted for annealing temperature of 1000 °C. This blue-shift may be explained by considering the Moss–Burstein band filling effect [44]. It is well known that ZnO is an n-type semiconductor and so the Fermi level is inside the conduction band. It is evident from the PL spectra that oxygen vacancies enhanced at 900 °C due to Mg doping and hence there is further increase in the n-type nature of ZnO. As a result of it the Fermi level of ZnO shifts to higher level due to high concentration of electrons in the conduction band at 1000 °C. Consequently, electrons in the valence band excited to the Fermi level which is well above the conduction band edge and absorption spectrum is blue-shifted. Hence, the decrease of green emission intensity at 1000 °C may be due to the deterioration of the crystal quality.

3.3.4. *Energy level diagram model*

Moreover, various transition mechanisms have been proposed for the green emission which includes transition of an electron from conduction band to the deep acceptor (V_o) [35] and transition of an electron from shallow donor to the deep acceptor [36]. To understand, the transitions involved in the green emission observed in this study, the PL Excitation (PLE) spectra were recorded by monitoring the emission wavelengths at 396 nm and 503 nm. Fig. 9 shows the PLE spectra of ZnO–MgO nanocomposite (annealed at 900 °C) acquired by monitoring the emission wavelengths at 396 nm and 503 nm. Fig. 9 shows a sharp and weak peak centered at 353 nm when emission wavelength is monitored at 396 nm and a broad and intense peak at 353 nm when emission wavelength is monitored at 503 nm. It indicates that the top level for both the emissions is same i.e electrons are de-excited from the same excited state to different lower energy levels to produce UV and green emissions. The band gap of ZnO is 3.37 eV and the UV emission has been observed at 396 nm (3.13 eV). The energy difference between the near band edge emission and the UV emission at 3.13 eV is 0.24 eV. It is well established that the defect level due to the Zn_i lies 0.22 eV below the conduction band in ZnO [37,45] and it is in good agreement with the energy difference (0.24 eV) calculated above. Hence, it can be concluded that the emission at 396 nm is

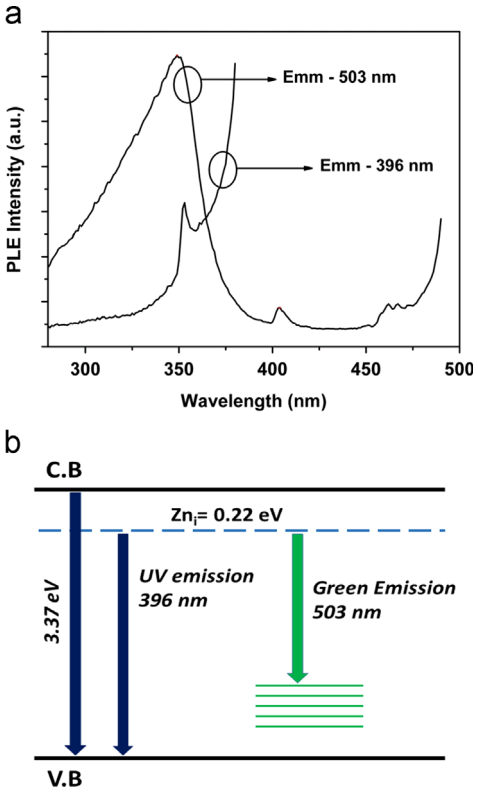

Fig. 9. (a) The PL Excitation spectra of ZM3 nanocomposite annealed at 900 °C acquired by monitoring the emission wavelengths at 396 nm and 503 nm and (b) energy level diagram indicating the transitions responsible for UV and green emissions.

originated due to the transition of an electron from Zn_i defect level below the conduction band to the valence band. On the other hand, theoretical and experimental investigations confirmed that oxygen vacancy (V_o) defect state is a deep level in the band gap of ZnO and it was calculated to be 0.5–0.8 eV above the conduction band maximum [46]. From Fig. 6 the excited state for green emission also lies 0.24 eV below the conduction band. The energy of green emission corresponding to the 503 nm is 2.46 eV and hence the oxygen vacancy defects responsible for the green emission should lie 0.67 eV above the valance band. It is in good agreement with the established fact that oxygen vacancy defect level lies 0.5–0.8 eV above the valence band maximum. So, the green emission observed in this study centered at 503 nm is assigned to the transition of an electron form shallow donor (defect level of Zn_i) to the deep acceptor (defect level of V_o).

4. Conclusion

In summary, structural and PL properties of ZnO–MgO nanocomposite prepared through sol–gel method were investigated. It was observed that ZnO nanocrystals are under strain with increase of Mg concentration in the ZnO–MgO nanocomposite. The UV emission intensity also enhanced with increase of Mg concentration and there exist a critical concentration beyond which there is no rise in the UV intensity. As the temperature increased from 600 °C to 900 °C, intensity of the green emission positioned at 503 nm increased and subsequently decreased for annealing at 1000 °C. The green emission is quenched completely when annealed in oxygen gas. It was also found that the intensity of the green emission depends on the concentration of Mg in ZnO–MgO nanocomposite. It was found by correlating the XRD and PL results of the annealed samples that the green emission is originated due to the diffusion of Mg atoms at the interface of ZnO and MgO. The diffusion of Mg atoms at the interface of ZnO and MgO created defects levels on the

interface. The electrons are trapped at these deep trap levels and give rise to the green emission. The decrease of green emission intensity at 1000 °C is presumed to be due to the deterioration of the crystal structure due to the formation of Zn_i defects. The increase of the band gap at 1000 °C is due to the Moss–Burstein effect. The green emission observed in this study centered at 503 nm is assigned to the transition of an electron form shallow donor (defect level of Zn_i) to the deep acceptor (defect level of V_o).

Acknowledgments

Authors grateful to Prof. T. P. Radhakrishnan, Department of Chemistry, Faculty Incharge of HR-TEM, University of Hyderabad for providing the HR-TEM measurements of our samples. Authors also thankful to Dr. Paul Joseph Daniel, Assistant Professor, Department of Physics, NIT Warangal, for his valuable suggestions.

Appendix A. Supporting information

Supplementary data associated with this article can be found in the online version at http://dx.doi.org/10.1016/j.jlumin.2014.10.027.

References

[1] C.Y. Liu, H.Y. Xu, J.G. Ma, X.H. Li, X.T. Zhang, Y.C. Liu, R. Mu, Appl. Phys. Lett. 99 (2011) 063115.
[2] D.C. Look, Mater. Sci. Eng. B 80 (2001) 383.
[3] T. Minami, T. Miyata, Y. Ohtani, Y. Mochizuki, Jpn. J. Appl. Phys. 45 (2006) L409.
[4] A. Nuruddin, J.R. Abelson, Thin Solid Films 394 (2001) 48.
[5] G.P. Dransfield, Radiat. Prot. Dosim. 91 (2000) 271.
[6] D.R. Clarke, J. Am. Ceram. Soc. 82 (1999) 485.
[7] J.F. Wager, Science 300 (2003) 1245.
[8] G.A. Prinz, Science 282 (1998) 1660.
[9] A. Van Dijken, E.A. Meulenkamp, D. Vanmaekelbergh, A. Meijerink, J. Phys. Chem. B 104 (2000) 1715.
[10] K. Vanheusden, W.L. Warren, C.H. Seager, D.R. Tallent, J.A. Voigt, B.E. Gnade J. Appl. Phys. 79 (1996) 7983.
[11] B. Guo, Z.R. Qiu, K.S. Wong, Appl. Phys. Lett. 82 (2003) 2290.
[12] A. Sharma, S. Dhar, B.P. Singh, Appl. Surf. Sci. 273 (2013) 144.
[13] X.H. Huang, C. Zhang, C.B. Tay, T. Venkatesan, S.J. Chua, Appl. Phys. Lett. 102 (2013) 111106.
[14] S. Panigrahi, D. Basak, J. Colloid Interf. Sci. 353 (2011) 30.
[15] J. Li, D. Zhao, X. Meng, Z. Zhang, J. Zhang, D. Shen, Y. Lu, X. Fan, J. Phys. Chem. B 110 (2006) 14685.
[16] C. Jin, H. Kim, H.Y. Ryu, H.W. Kim, C. Lee, J. Phys. Chem. C 115 (2011) 8513.
[17] J.P. Richter, T. Voss, D.S. Kim, R. Scholz, M. Zacharias, Nanotechnology 19 (2008) 305202.
[18] P. Shimpi, P.X. Gao, D.G. Goberman, Y. Ding, Nanotechnology 20 (2009) 125608.
[19] D. Bera, L. Qian, P.H. Holloway, J. Phys. D: Appl. Phys. 41 (2008) 182002.
[20] N.O.V. Plank, H.J. Snaith, C. Ducati, J.S. Bendall, L. Schmidt-Mende M.E. Welland, Nanotechnology 19 (2008) 465603.
[21] I. Kaminska, B. Sikora, K. Fronc, P. Dziawa, K. Sobczak, R. Minikayev, W. Paszkowicz, D. Elbaum, J. Phys.: Condens. Matter 25 (2013) 194105.
[22] K. Vijayalakshmi, K. Karthick, P. Deepak Raj, M. Sridhara, Ceram. Int. 40 (2014) 827.
[23] X.Q. Meng, H. Peng, Y.Q. Gai, J. Li, J. Phys. Chem. C 114 (2010) 1467.
[24] Z. Fu, W. Dong, B. Yang, Z. Wang, Y. Yang, H. Yan, S. Zhang, J. Zuo, M. Ma, X. Liu, Solid State Commun. 138 (2006) 179.
[25] Y.J. Zeng, Z.Z. Ye, F. Liu, D.Y. Li, Y.F. Lu, W. Jaeger, H.P. He, L.P. Zhu, J.Y. Huang B.H. Zhao, Cryst. Growth Des. 9 (2009) 263.
[26] C. Jin, H. Kim, H. Ryu, H.W. Kim, C. Lee, Curr. Appl. Phys. 11 (2011) S60.
[27] H.Y. Yang, S.F. Yu, G.P. Li, T. Wu, Opt. Express 18 (2010) 13647.
[28] J. Bang, H. Yang, P.H. Holloway, Nanotechnology 8 (2006) 973.
[29] K. Sowri Babu, A. Ramachandra Reddy, K. Venugopal Reddy, Mater. Res. Bull. 45 (2014) 1368.
[30] J. Cao, J. Yang, L. Yang, M. Wei, B. Feng, D. Han, L. Fan, B. Wang, H. Fu, J. Appl. Phys. 112 (2012) 014316.
[31] A.M. Smith, A.M. Mohs, S. Nie, Nat. Nanotechnol. 4 (2009) 56–63. http://dx.doi.org/10.1038/NNANO.2008.360.
[32] K. Sowri Babu, A. Ramachandra Reddy, C.H. Sujatha, K. Venugopal Reddy, Optimization of UV emission intensity of ZnO nanoparticles by changing the excitation wavelength, Mater. Lett. 99 (2013) 97–100.
[33] K. Sowri Babu, A. Ramachandra Reddy, C.h. Sujatha, K. Venugopal Reddy A.N. Mallika, Mater. Lett. 110 (2013) 10.
[34] H.W. Kim, H.S. Kim, C. Lee, M.A. Kebede, K.H. Yoo, D.Y. Kim, J. Korean Phys. Soc. 55 (2009) 1887.
[35] W.C. Zhang, X.L. Wu, H.T. Chen, J. Zhu, G.S. Huang, J. Appl. Phys. 103 (2008) 093718.
[36] A.B. Djuriˇsic, Y.H. Leung, K.H. Tam, L. Ding, W.K. Ge, H.Y. Chen, S. Gwo, Appl. Phys. Lett. 88 (2006) 103107.
[37] H.B. Zeng, G.T. Duan, Y. Li, S.K. Yang, X.X. Xu, W.P. Cai, Adv. Funct. Mater. 20 (2010) 561.
[38] J.J. Lee, J. Bang, H. Yang, J. Phys. D: Appl. Phys. 42 (2009) 025305.
[39] J.D. Ye, S.L. Gu, S.M. Zhu, W. Liu, S.M. Liu, R.Z hang, Y. Shi, Y.D. Zheng, Appl. Phys. Lett. 88 (2006) 182112.
[40] G.K. Williamson, W.H. Hall, Acta Metall. 1 (1953) 22.
[41] W.Q. Peng, S.C. Qu, G.W. Cong, Z.G. Wang, Appl. Phys. Lett. 88 (2006) 101902.
[42] A. Ohtomo, R. Shiroki, I. Ohkubo, H. Koinuma, M. Kawasaki, Appl. Phys. Lett. 75 (1999) 4088.
[43] R. Dutta, N. Mandal, Appl. Phys. Lett. 101 (2012) 042106.
[44] S. Suwanboon, P. Amornpitoksuk, A. Sukolra, Ceram. Int. 37 (2011) 1359.
[45] T. Prasada Rao, G.K. Goswami, K.K. Nanda, J. Appl. Phys. 115 (2014) 213513.
[46] M.D. McCluskey, S.J. Jokela, J. Appl. Phys. 106 (2009) 071101.